LAWRENCE
LIVERMORE
NATIONAL
LABORATORY

LLNL-JRNL-660982

Iterative Implicit Monte Carlo

N. Gentile, B. Yee

September 23, 2014

Journal of Computational and Theoretical Transport

Disclaimer

Journal of Computational and Theoretical Transport

ITERATIVE IMPLICIT MONTE CARLO

N. A. Gentile
Lawrence Livermore National Laboratory L-38
7000 East Avenue
Livermore, CA 94551
gentile1@llnl.gov
and

Ben C. Yee
Department of Nuclear Engineering & Radiological Sciences
University of Michigan
1928 Cooley Building
2355 Bonisteel Boulevard
Ann Arbor, Michigan USA 48109-2104

ABSTRACT

We describe a new Monte Carlo thermal radiation transport method that is fully implicit in the value of matter termperature used to calculate thermal emission. This method involves iterating on the matter temperature until convergence at the time $n+1$ value of the matter temperature is obtained. Because the method is fully implicit, it eliminates the violations of the maximum principle that can occur in Implicit Monte Carlo (IMC) simulations on the problems on which we have tested it. The method has the drawback that it is considerably more expensive than IMC for simulations with cold opaque regions. We discuss the reasons for this, and discuss some ways that the number of iterations may be reduced.

Key Words: thermal radiation transport, Monte Carlo methods.

1. INTRODUCTION

The time-dependent frequency-dependent transport equation for photons is [1]

$$\frac{1}{c}\frac{\partial I}{\partial t}+\Omega\cdot\nabla I = -\sigma_t(T,\nu)I+\sigma_a(T,\nu)B(T,\nu)+\int_0^\infty\int_{4\pi}\mathrm{d}\nu'\mathrm{d}\Omega'\;\sigma_s(T,\nu,\nu')I(x,t,\nu',\Omega')+S_r(x,t,\nu,\Omega) \tag{1}$$

where $I(x,t,\nu,\Omega)$ is the radiation intensity, with units of energy/(length^2 frequency solid angle), c is the speed of light, T is the material temperature, $\sigma_a(T,\nu)$ is the macroscopic absorption opacity in inverse length units, $\sigma_s(T,\nu)$ is the macroscopic scattering opacity in inverse length units, and $\sigma_t(T,\nu)=\sigma_a(T,\nu)+\sigma_s(T,\nu)$. $B(\nu,T)$ is the Planck function and $S_r(x,t,\nu,\Omega)$ is a time and space-dependent radiation source. This equation comes with initial conditions $I_{ic}(x,t,\Omega)$ defined for all points in the region of interest, and boundary conditions $I_{bc}(x,t,\Omega)$ defined on the boundary of the region of interest for values of Ω that ensure that I_{bc} describes incoming photons. The Planck function is defined via

$$B(T,\nu)\equiv\frac{2h\nu^3}{c^2}\frac{1}{e^{\frac{h\nu}{kT}}-1} \tag{2}$$

where h is Planck's constant and k is Boltzmann's constant. $B(T,\nu)$ satisfies

$$\int_0^\infty \mathrm{d}\nu\ B(T,\nu) = \frac{1}{4\pi} acT^4\ , \tag{3}$$

where $a = \frac{8\pi^5 k^4}{15c^3h^3}$ is the radiation constant. The thermal emission term, σB, can be written

$$\sigma_a(T,\nu)B(T,\nu) = \frac{1}{4\pi}\frac{\sigma_a(T,\nu)b(T,\nu)}{\sigma_P(T)}\sigma_P(T)acT^4 \tag{4}$$

where a is the radiation constant, T is the matter temperature, $b(T,\nu)$ is the Planck distribution normalized over frequency, defined by

$$b(T,\nu) \equiv \frac{15}{\pi^4}\frac{(\frac{h\nu}{kT})^3\frac{h}{kT}}{\exp(\frac{h\nu}{kT})-1}, \tag{5}$$

and σ_P is the Planck mean opacity

$$\sigma_P(T) = \int_0^\infty \mathrm{d}\nu\ \sigma_a(T,\nu)b(T,\nu). \tag{6}$$

The expression $\frac{\sigma_a(T,\nu)b(T,\nu)}{\sigma_P(T)}$ is the probability distribution function for the frequency of the thermally emitted photons.

The transport equation is coupled to the material energy balance equation [1]

$$\frac{\partial e_m}{\partial t} = \rho c_v \frac{\partial T}{\partial t} = \int_0^\infty \mathrm{d}\nu \int_{4\pi} \mathrm{d}\Omega\ \sigma_a I - c\sigma_P aT^4\ . \tag{7}$$

Here, $e_m(\rho,T)$ is the equation of state, which gives the matter energy density in units of energy per volume as a function of the mass density and temperature, ρ is the mass density, and c_v is the heat capacity in units of energy per mass per temperature. We assume, here and henceforth, that ρ is constant in time.

Eqs.(1) and (7) are often solved by Monte Carlo methods. These methods advance solutions of Eqs.(1) and (7) over a time interval $[t_n, t_n + \Delta t]$ that is small enough that we can regard σ_a and σ_s as fixed at their t_n values. Even for small values of Δt, however, it is not possible to use $T(t_n)$ in the thermal emission term without encountering instabilities [2]. Eliminating these instabilities is the reason for the development of the Implicit Monte Carlo (IMC) algorithm [3]. IMC uses a semi-implicit approximation to get an estimate of the matter temperature at $t_n + \Delta t$ [4]. The effect of this approximation is to modify Eqs.(1) and (7) by multiplying the absorption opacity by a factor

$$f_a = \frac{1}{1+\beta c\Delta t\sigma_P} \tag{8}$$

and adding an equal amount of thermally redistributed isotropic scattering. Here $\beta \equiv 4aT^3/\rho c_v$. Since all the quantities in the denominator are positive, we have $f_a \in (0,1]$. The quantity f_a defined by Eq. (8) is sometimes referred to as the "Fleck factor". Although the instabilities are eliminated by the Implicit Monte Carlo method described in [3], thermodynamically inconsistent matter and radiation temperatures can still result in simulations with large values of Δt [7].

In this work, we describe a new iterative Monte Carlo method, which we call Iterative Implicit Monte Carlo (IIMC). This method is an iterative one which allows us to estimate the value of $T(t_{n+1})$ used in calculating thermal emission more accurately than the semi-implicit approximation used in [3] does. This method does not employ effective scattering; the unmodified t_{n+1} values of σ_a and σ_s are used. This method eliminates thermodynamically inconsistent values of the temperature, at the sometimes prohibitive cost of running many more particles to describe thermal emission at various intermediate temperatures.

2. SEPERATING OUT THE THERMAL PART OF THE TRANSPORT EQUATION

We can take advantage of the linearity of Eq.(1) in I to separate it into 3 parts, only one of which contains the non-linear term in T. We represent I as the sum of three quantities, $I_c + I_s + I_t$. These quantities model the photons that result from the initial conditions, the radiation sources and boundary conditions, and the thermal emission respectively. In what follows, we will assume that we can use t_n values of the opacity, but we will use an estimate of the t_{n+1} value of the temperature for thermal emission.

First, we will model the effects of the initial conditions. We will chose I_c to satisfy the equation

$$\frac{1}{c}\frac{\partial I_c}{\partial t} + \Omega \cdot \nabla I_c = -\sigma_t(T_n, \nu) I_c + \int_0^\infty \int_{4\pi} d\nu' d\Omega' \; \sigma_s(T_n, \nu, \nu') I_c \tag{9}$$

with the initial condition $I_c(t_n) = I_{ic}$ and boundary condition $I_c = 0$ on the boundary of the region of interest. Note that, because we have fixed the opacities at their value at t_n, this equation is independent of T. In the first time step, I_{ic} describes the initial conditions of the problem. In subsequent time steps, it describes the value of I at the end of the previous time step. In a Monte Carlo simulation, I_{ic} would be represented by the census particles from the previous time step.

Next, we will model the effects of any radiation sources. We will chose I_s to satisfy the equation

$$\frac{1}{c}\frac{\partial I_s}{\partial t} + \Omega \cdot \nabla I_s = -\sigma_t(T_n, \nu) I_s + \int_0^\infty \int_{4\pi} d\nu' d\Omega' \; \sigma_s(T_n, \nu, \nu') I_s + S_r(x, t_n, \nu, \Omega) \tag{10}$$

with initial condition $I_s(t_n) = 0$ and boundary condition $I_s = I_{bc}$ on the boundary of the region of interest. Note that this equation, like Eq.(9), is independent of T.

We determine the equation satisfied by I_t by inserting $I_c + I_s + I_t$ into Eq.(1) and subract Eqs.(9) and (10) from it. The result is

$$\frac{1}{c}\frac{\partial I_t}{\partial t} + \Omega \cdot \nabla I_t = -\sigma_t(T_n, \nu) I_t + \sigma_a(T_n, \nu) B(T_{n+1}, \nu) + \int_0^\infty \int_{4\pi} d\nu' d\Omega' \; \sigma_s(T_n, \nu, \nu') I_t \tag{11}$$

with initial condition $I_t(t_n) = 0$ and boundary condition $I_t = 0$ on the boundary of the region of interest. This equation models the effects of thermally emitted photons. Unlike Eqs.(9) and (10), this equation contains the non-linear term in T.

Written in terms of I_c, I_s, and I_t, Eq.(7) becomes

$$\frac{\partial e_m}{\partial t} = \int_{4\pi} \mathrm{d}\Omega \int_0^\infty \mathrm{d}\nu \; \sigma_a (I_c + I_s + I_t) - c\sigma_P a [T_{n+1}]^4 \tag{12}$$

Solving Eqs.(9) and (10) by Monte Carlo is straightforward because they do not depend on the unknown value T_{n+1}. To solve Eq.(9), we create Monte Carlo particles representing the photons described by I_{ic} and t_n and track their progress until $t + \Delta t$ is reached, simulating scatters and boundary exits and tallying the energy absorbed for later use in Eq.(12). Solving Eq.(10) is done in a similar manner, the only difference being that Monte Carlo particles are created during the time step and on the boundaries with times, energies, positions and directions drawn from distributions derived from the boundary conditions I_{bc} and the source S_r. Solving these equations gives us the values of I_c and I_s at time $t_{n+1} \equiv t_n + \Delta t$. At the beginning of the next time step, we use $I_{ic}(t_{n+1}) = I_c(t_{n+1}) + I_s(t_{n+1}) + I_t(t_{n+1})$ to solve Eqs.(9) and (10) from t_{n+1} to $t_{n+1} + \Delta t_{n+1}$. Note that, in solving Eqs.(9) and (10) we are not using the effective scattering that would be present in the Fleck and Cummings method [3].

This leaves only the problem of solving Eq.(11) for $I_t(t)$ and Eq.(12) for $T(t_{n+1})$. We will describe a technique for doing so in the next section.

3. A SERIES SOULTION FOR I_t

One way of eliminating thermodynamically inconsistent values of T is to iterate on the value of T used in the in emission source term in Eqs.(1) and (7). This is called Picard iteration. This technique requires repeated solution of Eq.(1) using values of T that come from previous iterations, and then solving Eq.(7) to obtain an updated value of T. The first iteration uses the value of T at t_n. Subsequent iterations use the final value of T obtained from the previous iteration. This iterative technique produces a sequence of values of I^i and T^i, with I^i a function of T^{i-1}. As i is increased, we hope that I^i and T^i converge. Note that, in this scheme, all of the particles generated using the T^i, except for the particles generated using the last value, are terminated and are not put into census.

This technique is often used by deterministic transport schemes; frequently, some sort of acceleration technique is also used. It is not commonly used with Monte Carlo because of the expense of multiple solutions of the transport equation, and the expense of storing the beginning of time step value of I. (In a Monte Carlo simulation, I is represented as a collection of particles, and we would have to keep a copy of this set, representing $I(t_n)$, to use as the initial value of I for each iteration.)

In this section, we will develop a similar solution technique to solve Eq.(11). However, we are going to replace the sequence of solutions that result from Picard iteration with a series solution:

$$I_t = I_t^0 + I_t^1 + ... + I_t^i + ... = \sum_{i=0}^{\infty} I_t^i \ . \tag{13}$$

We will hope that the series converges. In practice, we will monitor the values of I_t^i and terminate the series when these values are acceptably small.

For notational convenience, we are going to define the transport operator $\mathcal{T}(I)$:

$$\mathcal{T}(I) \equiv \frac{1}{c}\frac{\partial I}{\partial t} + \Omega \cdot \nabla I + \sigma_t(T_n, \nu) I - \int_0^\infty \int_{4\pi} d\nu' d\Omega' \ \sigma_s(T_n, \nu, \nu') I \tag{14}$$

Note that $\mathcal{T}$ is linear in I. This definition allows us to write Eq.(11) as

$$\mathcal{T}(I_t) = \sigma_a(T_n,\nu)B(T_{n+1},\nu) = \frac{1}{4\pi}\sigma_a(T_n,\nu)b(T_{n+1},\nu)ac(T_{n+1})^4 \tag{15}$$

The term on the right-hand side of Eq.(15) describes thermal emission. Both $\sigma_a(T,\nu)$ and $b(T,\nu)$ depend on the frequency and temperature. This means that these two terms allow us to calculate the temperature-dependent probability distribution function for the frequency of the emitted photons, as well as the total amount of energy that is emitted. For numerical convenience, we can remove the temperature dependence of the probability distribution function for the frequency by fixing both the opacity σ_a and the normalized Planck function b at the initial temperature T^n. This approximation is used, for example, in the IMC method [3]. We will use it below, because we will be sampling the thermal emission in an iterative way, and we wish to avoid calculating a new probability distribution function for each iteration. This means that we will replace Eq.(15) with this equation

$$\mathcal{T}(I_t) = \frac{1}{4\pi}\sigma_a(T_n,\nu)b(T_n,\nu)ac(T_{n+1})^4 \ . \tag{16}$$

In Eq.(16), the frequency distribution of the thermally emitted particles is centered at t_n, but the magnitude of the energy emitted is the correct T_{n+1} value.

The first step in the series solution of Eq.(13) is to solve for I_c via Eq.(9) and I_s via Eq.(10) as described in the last section. That leaves us with Eqs.(11) and (12). From our solutions to Eqs.(9) and (10), we know the integrals over angle and frequency of $\sigma_a I_c$ and $\sigma_a I_s$ in Eq.(12). The only unknowns are I_t and T.

The second step is to represent I_t with Eq.(13). This gives us

$$\mathcal{T}\left(\sum_{i=0}^{\infty} I_t^i\right) = \sum_{i=0}^{\infty}\mathcal{T}(I_t^i) = \frac{1}{4\pi}\sigma_a(T_n,\nu)b(T_n,\nu)ac(T_{n+1})^4 \ , \tag{17}$$

with T_{n+1} satisfying

$$\frac{\partial e_m}{\partial t} = \int_{4\pi}\mathrm{d}\Omega\int_0^{\infty}\mathrm{d}\nu\ \sigma_a(T_n,\nu)(I_c+I_s) + \sum_{i=0}^{\infty}\int_{4\pi}\mathrm{d}\Omega\ \int_0^{\infty}\mathrm{d}\nu\ \sigma_a(T_n,\nu)I_t^i - c\sigma_P(T_n)a(T_{n+1})^4 \ . \tag{18}$$

Since we have introduced new degrees of freedom (the I_t^i), Eqs.(17) and (18) do not determine the value of the I_t^i individually; they only constrain their sum I_t. The third step in our solution technique is to introduce some further equations to constrain the values of the I_t^i. This is done by representing the temperature source with a sequence of values T^i. We choose the I_t^i individually to satisfy

$$\begin{aligned}
\mathcal{T}(I_t^0) &= \frac{1}{4\pi}\sigma_a(T_n,\nu)b(T_n,\nu)ac(T^0)^4 \\
\mathcal{T}(I_t^1) &= \frac{1}{4\pi}\sigma_a(T_n,\nu)b(T_n,\nu)ac[(T^1)^4-(T^0)^4] \\
&\ldots \\
\mathcal{T}(I_t^i) &= \frac{1}{4\pi}\sigma_a(T_n,\nu)b(T_n,\nu)ac[(T^i)^4-(T^{i-1})^4] \\
&\ldots
\end{aligned} \tag{19}$$

where we have not defined the T^i yet. The T^i in Eq.(19) are used only in determining the amount of energy that is thermally emitted in iteration i. Physical quantities such as σ_a and σ_s are evaluated at the T_n, the temperature at the beginning of the time step. Note that, as T^{i-1} approaches T^i, the magnitude of the thermal source term is reduced.

If the sequence of expressions in Eq.(19) are summed over i, the source terms cancel in pairs and leave us with

$$\mathcal{T}\left(\sum_{i=0}^{\infty} I_t^i\right) = \sum_{i=0}^{\infty} \mathcal{T}(I_t^i) = \frac{1}{4\pi}\sigma_a(T_n,\nu)b(T_n,\nu)ac(T^\infty)^4 \ , \tag{20}$$

where T^∞ is the value to which the sequence of T^i converges (assuming that the sequence does converge).

One property we would like the sequence of T^i to have is that it converges to T_{n+1}; that is, we would like $T^\infty = T_{n+1}$. T_{n+1} satisfies a backward Euler difference approximation to Eq.(18):

$$\begin{aligned} e_m(T_{n+1}) - e_m(T_n) &= \int_{t_n}^{t_n+\Delta t} \mathrm{d}t \int_{4\pi} \mathrm{d}\Omega \int_0^\infty \mathrm{d}\nu \ \sigma_a(I_c + I_s) \\ &+ \int_{t_n}^{t_n+\Delta t} \mathrm{d}t \int_{4\pi} \mathrm{d}\Omega \int_0^\infty \mathrm{d}\nu \ \sigma_a I_t - c\sigma_P a(T_{n+1})^4 \Delta t \ . \end{aligned} \tag{21}$$

If T^i does converge to T_{n+1}, then the solution of Eqs.(17) and (21) with an infinite number of terms would be a good approximation, first order in Δt, to Eqs.(11) and (12). We could then further hope that I_t^i and $T^i - T^{i-1}$ will become small as i increases, so that we could terminate the series at some finite value of i and take that finite series as an approximate solution to Eqs.(11) and (12).

Another desirable property for the T^i would be that they be monotonically increasing. That is, we would like $T^{i+1} > T^i$ for all i. This property would ensure that the source terms on the right-hand side of Eq.(17) would always be positive. Positivity is a desirable property for source terms in a Monte Carlo solution because it ensures that we will always have positive weight particles.

The fourth step in our approximation technique will be to define the sequence T^i in such a way that it has the two properties mentioned above. We do this by choosing the T^i to satisfy the following non-linear equation:

$$e_m(T^i) - e_m(T_n) = \int_{t_n}^{t_n+\Delta t} \mathrm{d}t \int_{4\pi} \mathrm{d}\Omega \int_0^\infty \mathrm{d}\nu \left[\sigma_a(I_c + I_s) + \sigma_a \sum_{j=0}^{i-1} I_t^j - c\sigma_P a(T^i)^4 \Delta t\right] \ . \tag{22}$$

This equation defines $e_m(T^i)$ to be $e_m(T_n)$ added to the amount of energy absorbed from the photons representing I_c and I_s and the amount of energy absorbed from the photons representing I_t^0 through I_t^{i-1}, minus the amount emitted at the temperature T^i. That is, we are calculating T_i to be the temperature we would obtain if a) the absorption from all initial and source photons is accounted for, b) the emission and absorption from all previous iterations of thermally emitted photons is accounted for, and c) the emission, but not the absorption, of photons from the current iteration are accounted for. This last point is crucial, because it ensures that $T_i < T_{i+1}$; this will be proved below.

As i increases, then (provided that I_t^i and $T^i - T^{i-1}$ are becoming small), Eq.(22) converges to Eq.(21). Thus this definition for T^i satisfies the first property we desire.

When we simulate the particles from iteration i, the amount of energy absorbed will be greater than zero, as long as we have $\sigma_a > 0$. Since σ_a and I_t^j are always greater than or equal to zero, the integral over I_t^j in Eq.(22) is always positive or zero. Since the integral term in Eq.(22) must be larger for $i+1$ than it is for i, the value we get for T^{i+1} must be greater than or equal to the value of T^i.

This can be proved directly by differentiating Eq.(22) with respect to the energy absorbed. If we define the energy emitted E_e as

$$E_e(T^i) \equiv c\sigma_P a (T^i)^4 \Delta t \tag{23}$$

and the energy absorbed E_a as

$$E_a(I_c, I_s, \sum_{j=0}^{i-1} I_t^j) \equiv \int_{t_n}^{t_n+\Delta t} \mathrm{d}t \int_{4\pi} \mathrm{d}\Omega \int_0^\infty \mathrm{d}\nu \; \sigma_a (I_c + I_s) + \int_{t_n}^{t_n+\Delta t} \mathrm{d}t \int_{4\pi} \mathrm{d}\Omega \int_0^\infty \mathrm{d}\nu \; \sigma_a \sum_{j=0}^{i-1} I_t^j \; , \tag{24}$$

then Eq.(22) can be written as

$$e_m(T^i) - e_m(T_n) = E_a - E_e(T^i) \; . \tag{25}$$

Then differentiating with respect to E_a yields

$$\frac{\partial e_m}{\partial T} \frac{\partial T^i}{\partial E_a} = 1 - 4c\sigma_P a (T^i)^3 \frac{\partial T^i}{\partial E_a} \Delta t \; . \tag{26}$$

Solving for $\frac{\partial T^i}{\partial E_a}$ yields

$$\frac{\partial T^i}{\partial E_a} \left[\frac{\partial e_m}{\partial T} + 4c\sigma_P a (T^i)^3 \Delta t \right] = 1 \; . \tag{27}$$

Since thermodynamics requires $\frac{\partial e_m}{\partial T} > 0$, and since $\sigma_P \geq 0$ and $T^i \geq 0$, the term in brackets is positive, and so Eq.(27) implies that $\frac{\partial T^i}{\partial E_a} \geq 0$. Since E_a increases as i increases, the sequence T^i is monotonically increasing, which is the second property we desire.

When Eq.(22) is solved for T^i, the integrals over I_c, I_s, and I_t^j for $j \in [0, i-1]$ are all known. This equation defines a value of T^i for every zone in the simulation. It may be solved by any convenient 1D root-finding technique.

4. COMPARISON TO OTHER MONTE CARLO THERMAL RADIATION TRANSPORT METHODS

In this section, we will compare the Iterative Implicit Monte Carlo method with some other Monte Carlo methods that have been employed for thermal radiative transport calculations.

First, we will discuss the Implicit Monte Carlo (IMC) method of Fleck and Cummings [3]. In IMC, stability is achieved by replacing a fraction f_a of the absorption by effective scattering. The "Fleck factor" f_a, lying in the range $[0, 1]$, is calculated as a function of temperature and

opacity, and this factor multiplies the absorption opacity and the thermal emission in both the transport equation and the material energy density equation. The effect of this is to replace a fraction of the absorption that takes place during the time step by scattering, called "effective scattering"; this "effective scattering" models absorption and re-emission. Because the amount of thermal emission is not calculated with the end of time step temperature T_{n+1}, the IMC method, while stable, can be thermodynamically inconsistent. For example, zones in a problem can reach a temperature higher than that of a Planckian source which is illuminating them. A negative consequence of effective scattering in very opaque problems is that the amount of effective scattering can be very large, which can increase the run time significantly. In contrast, the IIMC method does not have effective scattering. It achieves stability and thermodynamic consistency by modeling thermal emission at a close approximation of T_{n+1}, the value of which it achieves by iterating. More iterations are required when thermal emission dominates the energetics of a problem. This usually happens in problems with large opacities, which IMC would treat with a large amount of effective scattering. Thus, problems with a large opacity require many iterations, and can have larger run times than IMC.

Like the Symbolic Implicit Monte Carlo method (SIMC), [8], IIMC models thermal emission at T_{n+1}. In SIMC, this is achieved by using Monte Carlo particles to form a global linear or non-linear system that is solved for T_{n+1}. (Whether the global system is linear or non-linear depends on whether certain approximations for the time centering of the opacity and equation of state are employed.) IIMC replaces this global system with a series of local non-linear solves in each zone. SIMC only needs to simulate one set of thermally emitted particles, while IIMC runs many sets of thermally emitted particles, one set for each iteration, which it uses to form a series of approximations to T_{n+1}.

As SIMC does, we expect that IIMC would have increased "teleportation error" compared to IMC. The "teleportation error" is a spatial discretization error in the location of thermally emitted particles. Because we have a finite zone size, and, in most simulations, a piecewise linear spatial representation of the zonal temperature, we can select emission locations in a zone that are far away from where absorption actually occurred. (This can happen in zones that are more than a few mean free paths across.) This spatial inaccuracy can lead to thermal emission in parts of a zone that are not actually causally connected to a source, which in turn leads to an unphysically fast propagation of thermal waves. The effective scattering in IMC models absorption and re-emission at actual particle locations, and in IMC, thermal emission is reduced by the factor f. Both of these effects reduce, but do not eliminate, the "teleportation error". Because both IIMC and SIMC simulate all thermal emission by creating particles at sampled locations, both methods are subject to more "teleportation error" than IMC. In the problems simulated in this work, we have not seen evidence of more "teleportation error" than is present in IMC. We believe this is because we have not tried to simulate problems with zones that are optically thick enough. We expect this effect to appear in more challenging problems.

In [9], an iterative modified IMC algorithm that attempts to get a more accurate value of the opacity is described by Cheatham. That algorithm does this by a predictor-corrector methodology. An IMC simulation with a relatively small number of particles is run to get an estimate of the future matter temperature T_{n+1}. This is the predictor step. This estimate of T_{n+1} is then used to get an updated value of the opacity for another IMC simulation, the corrector step, the results of which are used as the final t_{n+1} values. Like IIMC, this method uses batches of particles, the results of which affect later batches. Unlike IIMC, the number of batches is fixed

at 2, and the first batch is thrown away - it does not contribute to census. The only part of the calculation that is affected by the first batch is the opacity. This method does not attempt to use the value of T_{n+1} obtained in the predictor step to calculate the amount of thermal emission. Thus, this method can exhibit the same thermodynamically inconsistent behavior as IMC, particularly in cases when the opacity is large but not a strong function of temperature.

Another iterative IMC method, called Iterative Thermal Emission IMC (ITE IMC), is described by Long, et. al. [10]. In this method, as in IIMC, the particles are run in several batches. The number of batches to be employed must be selected at the beginning of the time step. The amount of thermal emission, and the value of the Fleck factor, varies between batches, using information from previous batches. Since the Fleck factor varies, the amount of effective scattering varies between batches also. The ITE IMC method reduces the amount of violation of the maximum principle considerably compared to IMC. However, it does not eliminate it. It is a combination of semi-implicit steps, not a fully implicit method like IIMC.

5. A SIMPLE ANALYTIC EXAMPLE

A simple test problem that can be used to illustrate the behavior of IIMC is an infinite medium with a constant temperature $\hat{T}$, no source, σ_a a constant independent of ν, $\sigma_s = 0$, and an equation of state $e_m(T) = \gamma T^4$, with γ constant. Since σ_a is independent of frequency, $\sigma_P = \sigma_a$.

In this problem, there are no spatial or temporal derivatives and no angular dependence, so the solution of Eq.(1) is $I(\nu, \Omega) = B(\nu, \hat{T})$, and the solution of Eq.(7) is $e_m = \gamma \hat{T}^4$.

This problem can be analyzed over the interval $[t_n, t_n + \Delta t]$ in terms of I_c, I_s, and I_t. The initial conditions of the problem are $I_{ic} = B(\nu, \hat{T})$. Eq.(9) becomes

$$\frac{1}{c}\frac{\partial I_c}{\partial t} = -\sigma_a I_c \tag{28}$$

which has the solution $I_c(t) = B(\nu, \hat{T}) e^{-c\sigma_a(t-t_n)}$.

Since there is no source, $I_s(t) = 0$.

Eq.(11) becomes

$$\frac{1}{c}\frac{\partial I_t}{\partial t} = -\sigma_a I_t + \sigma_a B(T, \nu) \tag{29}$$

with $I_t(t_n) = 0$. This has the solution $I_t(t) = B(\nu, \hat{T})[1 - e^{-c\sigma_a(t-t_n)}]$. We see that, although neither $I_c(t)$ nor $I_t(t)$ are independent of time, $I_c(t) + I_t(t)$ equals the constant value $B(\nu, \hat{T})$ as required.

We will now apply the iterative solution technique described by Eqs.(19) and (22) to this problem.

$I_c(t)$ remains the same as in the analytic solution above. We require the value of the energy deposited by $I_c + I_s$ for Eq.(22). Using Eq.(3), that value can be calculated:

$$\begin{aligned} \int_{t_n}^{t_n+\Delta t} \mathrm{d}t \int_{4\pi} \mathrm{d}\Omega \int_0^\infty \mathrm{d}\nu \; \sigma_a (I_c + I_s) &= \int_{t_n}^{t_n+\Delta t} \mathrm{d}t \int_{4\pi} \mathrm{d}\Omega \int_0^\infty \mathrm{d}\nu \; \sigma_a B(\nu, \hat{T}) e^{-c\sigma_a(t-t_n)} \\ &= a\hat{T}^4[1 - e^{-c\sigma_a \Delta t}] \; . \end{aligned} \tag{30}$$

Using the equation of state, Eq.(22) becomes

$$\gamma(T^i)^4 - \gamma\hat{T}^4 = a\hat{T}^4[1 - e^{-c\sigma_a\Delta t}] + \int_{t_n}^{t_n+\Delta t} \mathrm{d}t \int_{4\pi} \mathrm{d}\Omega \int_0^\infty \mathrm{d}\nu\ \sigma_a \sum_{j=0}^{i-1} I_t^j - c\sigma_a a(T^i)^4\Delta t\ . \quad (31)$$

I_t^i is obtained from Eq.(19). For the infinite medium problem we are describing, the transport operator has the simplified form $\mathcal{T}(I) = \frac{1}{c}\frac{\partial I}{\partial t} + \sigma_a I$. From Eq.(19), we find that I_t^i satisfies

$$\frac{1}{c}\frac{\partial I_t^i}{\partial t} + \sigma_a I_t^i = \sigma_a[B(T^i) - B(T^{i-1})]\ . \quad (32)$$

Eq.(32) has the solution

$$I_t^i(t) = [B(\hat{T}^i) - B(\hat{T}^{i-1})][1 - e^{-c\sigma_a(t-t_n)}]\ . \quad (33)$$

which holds for $i = 0$ if we use the definition $T^{-1} \equiv 0$. I_t^i is independent of angle, as we expect in an infinite medium problem, because B is independent of angle.

It is convenient to define the energy density e_t^i associated with I_t^i:

$$e_t^i(t) \equiv \frac{1}{c}\int_{4\pi} \mathrm{d}\Omega \int_0^\infty \mathrm{d}\nu\ I_t^i \quad (34)$$

Using Eq.(3), we find that

$$e_t^i(t) = [a\ (T^i)^4 - a\ (T^{i-1})^4][1 - e^{-c\sigma_a(t-t_n)}]\ . \quad (35)$$

Integrating this expression over time yields

$$\int_{t_n}^{t_n+\Delta t} \mathrm{d}t\ e_t^i(t) = [a\ (T^i)^4 - a\ (T^{i-1})^4]\left[\Delta t - \frac{1}{c\sigma_a}[1 - e^{-c\sigma_a\Delta t}]\right]\ , \quad (36)$$

and thus

$$\sum_{j=0}^{i-1}\int_{t_n}^{t_n+\Delta t} \mathrm{d}t\ e_t^j(t) = a\ (T^{i-1})^4\left[\Delta t - \frac{1}{c\sigma_a}[1 - e^{-c\sigma_a\Delta t}]\right]\ , \quad (37)$$

Eq.(37) allows us to express the integral over I_t^i in Eq.(31) in terms of T^i. Then Eq.(31) can be solved for T^i, yielding

$$(T^i)^4 = \frac{\gamma + a[1 - e^{-c\sigma_a\Delta t}]}{\gamma + ac\sigma_a\Delta t}\hat{T}^4 + \frac{c\sigma_a\Delta t - [1 - e^{-c\sigma_a\Delta t}]}{\gamma + ac\sigma_a\Delta t}a(T^{i-1})^4\ . \quad (38)$$

The value of $(T^0)^4$ is

$$(T^0)^4 = \frac{\gamma + a[1 - e^{-c\sigma_a\Delta t}]}{\gamma + ac\sigma_a\Delta t}\hat{T}^4\ . \quad (39)$$

Eqs.(35) and (38) allow us to get the solution of the iterative method for any value of i. As $i \to \infty$, assuming that T^i converges, both T^i and T^{i-1} in Eq.(38) approach T^∞; solving Eq.(38) for T^∞ gives $T^\infty = \hat{T}$, as it must to agree with the analytic solution $T(t) = \hat{T}$.

These equations also give us some insight on when the method should converge quickly and when it will converge slowly. When γ is much larger than both a and $c\sigma_a\Delta t$, Eq.(39) implies

that $T^0 \approx \hat{T}$, and Eq.(38) implies that $T^i \approx T^{i-1}$. In this case, T^i converges quickly to $\hat{T}$. The first criterion means that the energy density of the material is large compared to the radiation energy density at T_i, and the second means that the fractional change in the radiation energy density e_t^i is small in the interval $[t_n, t_n + \Delta t]$, because that change is proportional to $e^{-c\sigma_a \Delta t}$ via Eqs.(30) and (37). In this situation, we would expect that the sequence of material temperatures T^i would not change much during the time step.

When $\gamma \gg a$ and $c\sigma_a \Delta t \gg 1$, then T^0 as given by Eq.(31) is small, and we expect convergence to be slow, as many cycles of emission and absorption will be necessary to build up enough thermally emitted photons so that $\sum_i I_t^i$ will reach the steady-state value $B(\nu, \hat{T})$. The first criterion means that the energy density of the material is small compared to the radiation energy density at T^i, and the second means that the the fractional change in the radiation energy density e_t^i is large the interval $[t_n, t_n + \Delta t]$.

This convergence behavior is shown by two specific examples. We use units where $a = c = 1$ and take $\hat{T} = 1$, $t_n = 0$ and $\Delta t = 1$. We examine two cases: case 1 has $\gamma = 1$, $\sigma_a = 1$ while case 2 has $\gamma = 10^{-4}$, $\sigma_a = 10^{10}$. For case 1, we expect rapid convergence of T^i to $\hat{T}$, while for case 2 we expect slower convergence. Fig. 1 shows T^i versus i for both cases. Fig. 2 shows

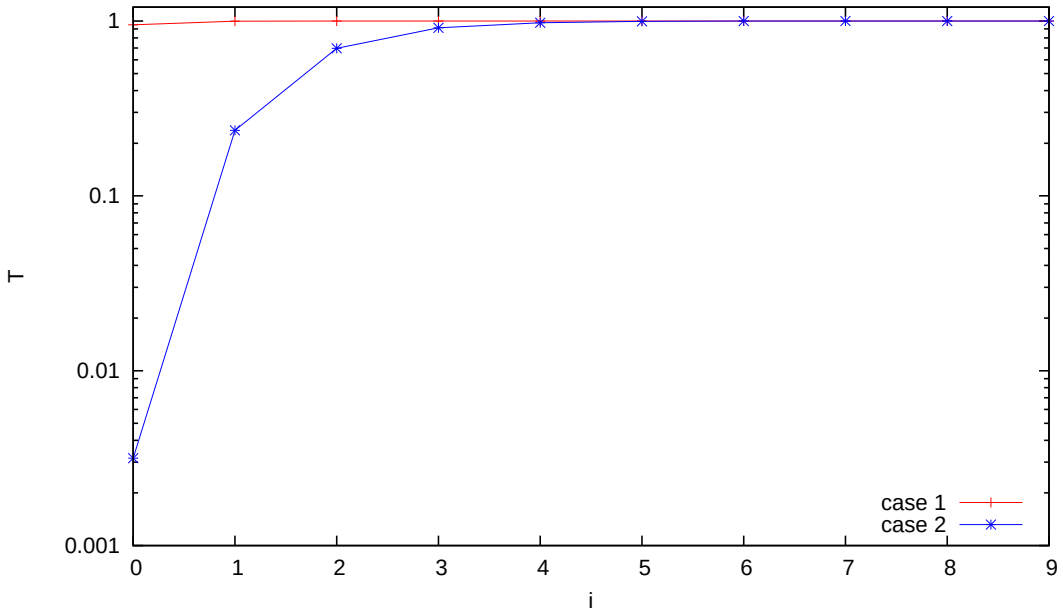

Figure 1: T^i computed from Eq.(31) versus iteration number i for the analytic problem described in Section 5. for two different values of γ and σ_a. Case 1 has $\gamma = 1$ and $\sigma_a = 1$ while case 2 has $\gamma = 10^{-4}$, $\sigma_a = 10^{10}$. Case 1 shows rapid convergence of T^i to $\hat{T}$, while case 2 shows slow convergence.

the energy density of census photons $e_c(t)$, the energy density of thermally emitted photons $\sum_{j=0}^{i} e_t^j(t)$, and the total radiation energy density $e(t)$, for a few different values of i over the interval $[0, \Delta t = 1]$ for case 1. We see that $e_c(t)$ declines relatively slowly over the time step, while $\sum_{j=0}^{i} e_t^j(t)$ converges after three iterations to the value given by Eq.(37). With $i = 2$, the total energy density is very close to the analytic value of $a\hat{T}^4 = 1$.

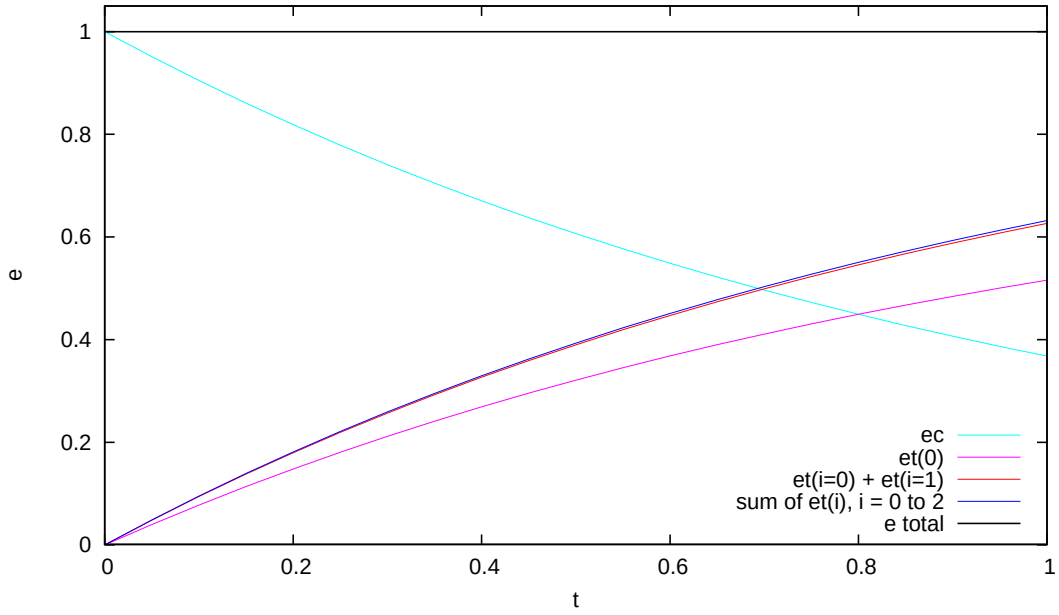

Figure 2: $e_c(t)$ and $\sum_{j=0}^{i}\ e_t^j(t)$ for case 1 of the analytic problem described in Section 5.. Case 1 has $\gamma = 1$, $\sigma_a = 1$. Case 1 shows rapid convergence of $e(t)$ to $\hat{T}$.

Fig. 3 shows $e_c(t)$, $\sum_{j=0}^{i}\ e_t^j(t)$, and $e(t)$ for a few different values of i over the initial part of the interval $[0, \Delta t = 1]$ for case 2. Because of the rapid decay of the energy in census photons, and the rapid increase in the thermal emission, we show only a part of the time interval. Because the census photons are quickly absorbed, the radiation energy density is dominated by thermally emitted photons for most of the interval. $\sum_{j=0}^{i}\ e_t^j(t)$ converges after three cycles. About seven iterations are necessary before the total energy density is very close to the analytic value of $a\ \hat{T}^4 = 1$.

We will see that convergence behavior of T^i for the infinite medium problem applies to the general case also. In Eq.(22) and Eq.(21), the integral over I_c and I_s represents the amount of energy absorbed from the initial and source photons, while the integral over I_t^i represents the amount of energy absorbed from thermally emitted photons. Comparing Eq.(22), which T^i satisfies, to Eq.(21), which T_{n+1} satisfies, we see that when the amount of absorption of the thermally emitted photons is large compared to the amount of absorption, $T^i \ll T^\infty$, and convergence will be slow. In the opposite case, $T^i \approx T^\infty$, and convergence will be fast. Simulations using more realistic equations of state and sources, and more than one zone, described in Section 7., will demonstrate this.

6. IMPLEMENTATION DETAILS

In the next section, we will describe the results of simulations performed using the IIMC method. In this section, we will give some details about our implementation of the algorithm.

IIMC was implemented in the IMC package of the Kull IMC code [5]. The Fleck factor was

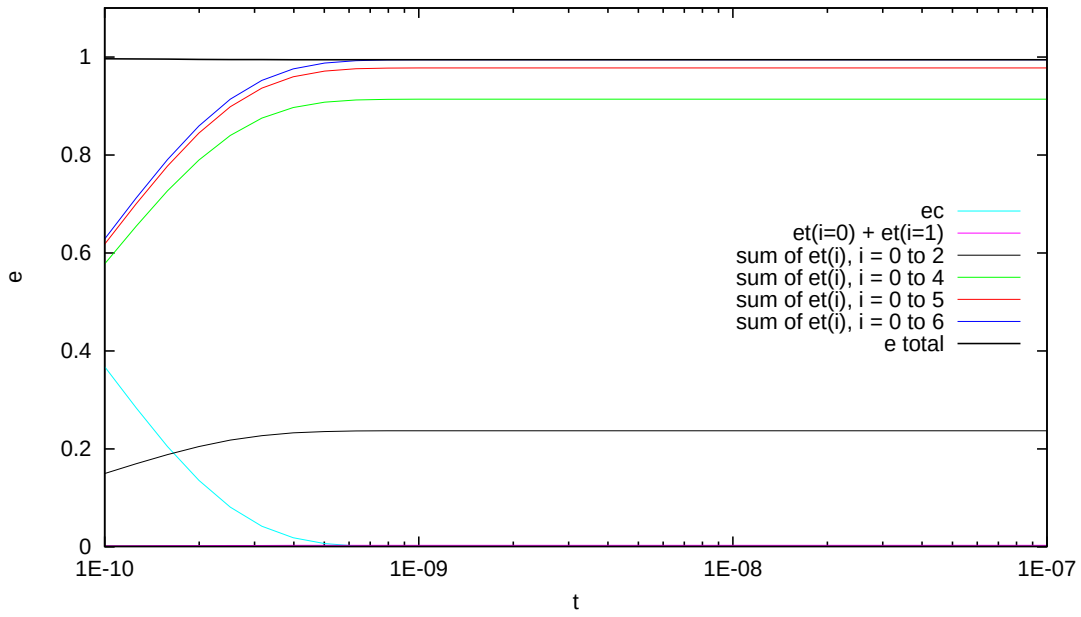

Figure 3: $e_c(t)$ and $\sum_{j=0}^{i}\ e_t^j(t)$ for case 2 of the analytic problem described in Section 5.. Case 2 has $\gamma = 10^{-4}$, and $\sigma_a = 10^{10}$. Case 2 shows very slow convergence of $e_t(t)$ to $\hat{T}$.

set to 1 in IIMC simulations by setting the parameter $\alpha = 0$ in Eq.(4.1d) of [3]. The routines that handle and track non-thermal source and census particles were the same as in IMC; these routines simulate Eqs.(9) and (10). The code was modified to allow multiple iterations of thermal source particles, simulating Eq.(19). The routine generating the thermal source particles had to be modified so that the amount of energy emitted was proportional to the difference of two Planckians, as in the right-hand side of Eq.(19). Simulating this equation also required the code to calculate a running tally of deposition, that is, the deposition from non-thermal source and census particles added to the deposition from previous iterations of thermal source particles. This quantity was necessary to calculate T^i via Eq.(21).

This non-linear equation was solved using Ridder's method [6]. We found that it was necessary to put a very strict convergence criterion on the method, because, for problems with a large opacity, a small change in T^i can lead to a large change in the values of the terms in Eq.(21). We required that the change in T^i to be less than 10^{-15} before accepting T^i as a solution to Eq.(21).

We will now describe the termination condition for the iteration of the thermal emission (that is, the termination of the iteration described by Eq.(19)). The iteration is terminated globally - all zones in the problem keep emitting while the iteration continues. We compute the magnitude of the thermally emitted energy in the current iteration summed over all the zones in the problem. We also keep a running sum over all iterations of the emission summed over all the zones in the problem. The iteration is terminated when the first quantity is less than 10^{-12} of the second.

That is, when

$$\sum_{z\in zones}\frac{1}{4\pi}\sigma_a(T_n,\nu)b(T_n,\nu)ac[(T^i)^4-(T^{i-1})^4] < 10^{-12}\sum_i\sum_{z\in zones}\frac{1}{4\pi}\sigma_a(T_n,\nu)b(T_n,\nu)ac[(T^i)^4-(T^{i-1})^4]\,. \tag{40}$$

We employed the same number of particles to model thermal emission for each iteration i. This choice was made purely for programing convenience. Since the amount of thermal emission in each iteration decreases as T^{i-1} approaches T^i, this means that the energy weight of the particles is decreasing as i increases. It is possible to reduce the number of particles representing thermal emission as the amount of thermally emitted energy decreases. This would presumably reduce the expense of the IIMC simulation.

7. NUMERICAL SIMULATIONS

7.1 Su-Olson volume source test problem

Su and Olson provided a semi-analytic solution for a one-dimensional, time-dependent, gray thermal radiative transport problem with a volume radiation source [11]. In this benchmark, which we will refer to as the Su-Olson problem, $a = c = \sigma_a = 1$ and $c_V = 4T_m^3$. At $x = 0$ there is a reflecting boundary and at large x there is a vacuum boundary. A volume radiation source with an emission rate of 1 per unit volume per unit time is located between $x = 0$ and $x = 0.5$, and is turned on between $t = 0$ and $t = 10$.

Results were obtained using IIMC and IMC with $\Delta t = 0.1$. The simulations used 1000 particles per IIMC cycle. Figure 4 shows that the computed material and radiation energy densities agree with the analytic solution. (For the earliest value of radiation energy density plotted in Figure 4, which occurs at $t = .1$, the value of calculated by IIMC is low compared to the analytic solution. This occurs because the radiation energy density is computed as an average over every particle path. This effectively centers the radiation energy density at the midpoint of the time step, rather than at the end. Thus, in Figure 4, we are comparing the simulation result at $t_n + \Delta t/2$ to the analytic value at time t_{n+1}. This difference is significant for the earliest result, which occurs after only one time step. For later results, it is less significant, which is why the later results show better agreement.)

Figure 5 shows how the number of IIMC iterations required in a time step changes over time. IIMC took 9 iterations in the initial time step and eventually converged to 5 IIMC iterations per time step. The total number of IIMC iterations was 564 and the run time was roughly 530 seconds on a single processor. This figure describes a simulation that took 100 time steps. (All simulations described in this paper were performed on 1 processor of a Linux cluster of 2.6 GHz Intel Xeon processors with 32 GB of memory per processor running Red Hat Linux.)

7.2 Infinite Medium Problem with T^{-3} Opacity

In this section an infinite medium problem with an opacity that scales as T^{-3} is considered. This problem has $c = a = 1.0$ and $\sigma_a = T^{-3}$. It was simulated using one zone with $\Delta x =$

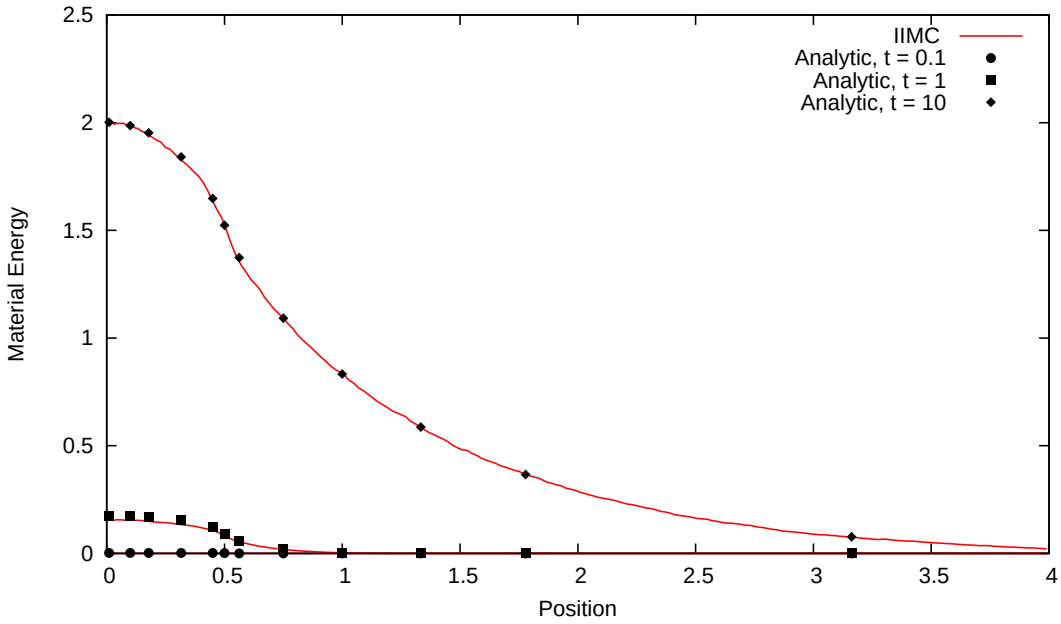

(a) Material energy density

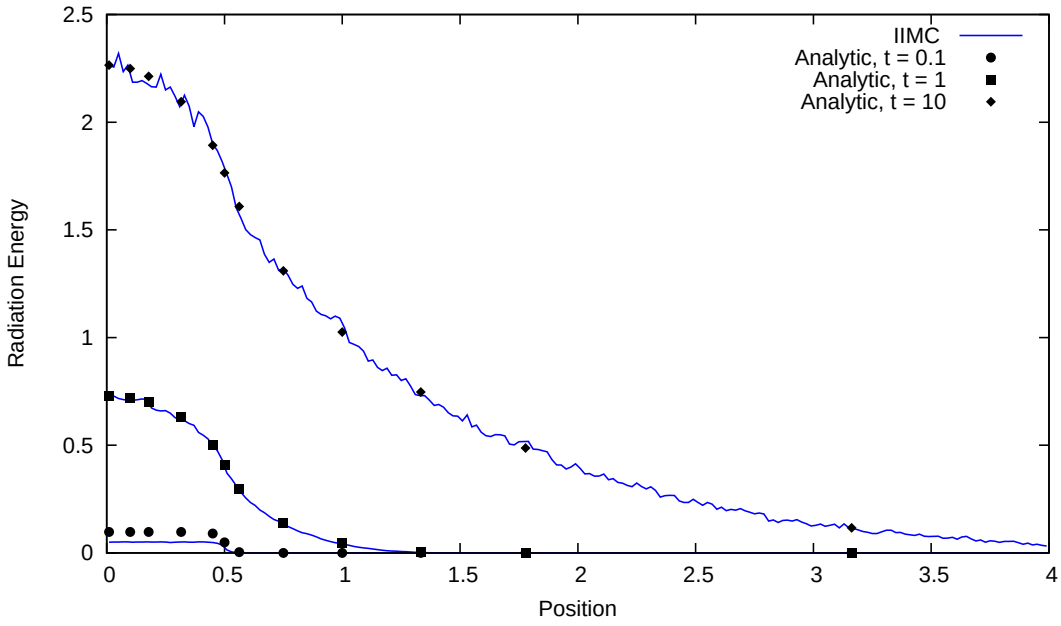

(b) Radiative energy density

Figure 4: Material and radiative energy densities vs. position at various times for the Su-Olson problem described in Section 7.1 using IIMC. The reference solution from [11] is also indicated on the plots.

$\Delta y = \Delta z = 1$ and reflecting boundaries on all faces. The initial conditions are $T_{m,0} = 0.1$ and $T_{r,0} = 1.0$. Figure 6 shows the results for time steps of $10^{-2}, 10^{-3}$ and 10^{-4} using both IMC and

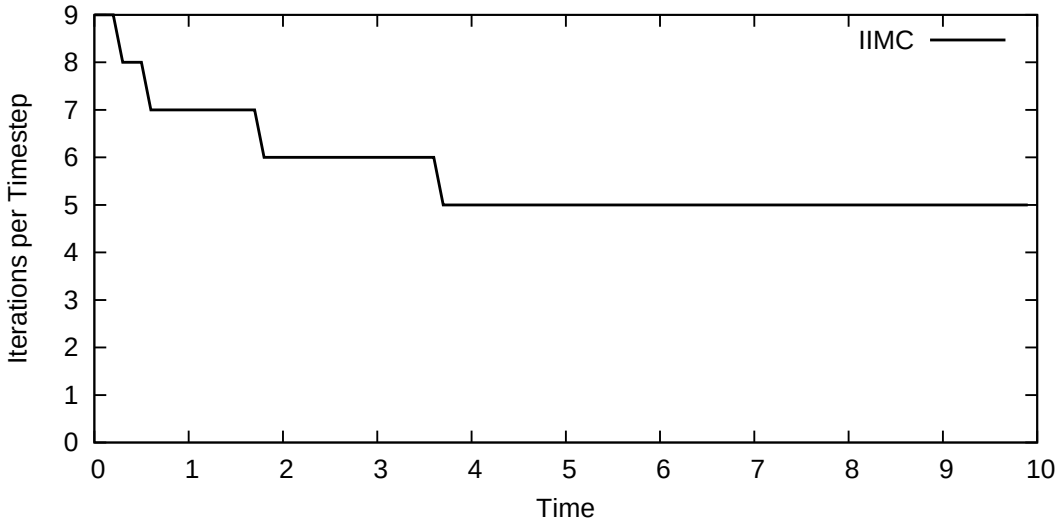

Figure 5: IIMC iterations per time step vs. time for the Su-Olson problem described in Section 7.1. IIMC needed a total of 564 iterations over the entire simulation (100 time steps) and had a runtime of approximately 530 seconds.

IIMC.

With $\Delta t = 10^{-4}$, we see that all three methods produce essentially the same result. This value of Δt is sufficiently small for all of the methods to resolve the changes in opacity and temperature. Both methods obtain the same result: temperature equilibrium is reached at approximately $t = 0.6$. As we increase Δt to 10^{-3}, we see that the IMC method becomes significantly less accurate than the IIMC method; the IMC results differ from the $\Delta t = 10^{-4}$ results more than the IIMC results do. With $\Delta t = 10^{-2}$, IMC violates the maximum principle. T_r exceeds T_m after one time step, and this situation is maintained for many time steps, because the large value of T_m causes σ_a to be so small that the rate of thermal emission is very small. This is not the case for IIMC. Although IIMC also degrades in accuracy as Δt increases, it does not degrade as seriously as the IMC method and it avoids violating the maximum principle. IIMC, being fully implicit, obtains the equilibrium solution in one time step when Δt becomes sufficiently large.

Table I summarizes the efficiency of the methods. The total run time over all time steps from $t = 0$ to $t = 1$, normalized to the number of particles generated by the simulation, is about the same for the two methods. Thus, the IIMC method is comparable in cost to the IMC method for this particular problem.

7.3 Face Source Problem

Here, we consider a one zone problem with a face source, material properties, and opacities similar to those of the the Marshak wave problem from Larsen and Mercier [7]. The problem features a radiation source on the left boundary at temperature $T_B = 1.0$ keV and an opacity which scales as T^{-3}. The left boundary is vacuum while the right boundary is reflective. The

Table I: Table summarizing run time characteristics of the IMC and IIMC methods for the infinite medium problem described in Section 7.2. The reported values are summed over all time steps for $t \in [0, 1]$. 1000 particles histories are simulated per IIMC iteration.

Δt	Method	Total IIMC Iterations	Run time (s)	Photons Created	$\frac{\text{Run time (s)}}{\text{Photons Created}}$
10^{-2}	IMC	—	84	1.94E+7	4.32E-6
10^{-2}	IIMC	557	306	6.54E+7	4.67E-6
10^{-3}	IMC	—	827	2.00E+8	4.14E-6
10^{-3}	IIMC	3015	1823	4.01E+8	4.54E-6
10^{-4}	IMC	—	8552	2.00E+9	4.28E-6
10^{-4}	IIMC	30003	17936	4.00E+9	4.49E-6

values of the other parameters are given by Table II. The domain runs between $x = 0$ cm and $x = 0.4$ cm and the mesh consists of just one spatial cell. This problem has a much higher opacity than the one described in the previous section. We use it to test the behavior of IIMC for problems with zones many mean free paths thick.

Table II: Parameter values for the face source problem.

$$\begin{aligned} \sigma_a(T) &= \tfrac{15}{\pi^4}\ \tfrac{27}{T^3}\tfrac{1}{\text{cm}}\ (T \text{ in keV}) \\ \rho c_V &= 8.1181 \cdot 10^{13}\ \tfrac{\text{erg}}{\text{keV cm}^3} \\ c &= 30.0\ \tfrac{\text{cm}}{\text{ns}} \\ a &= 1.372016 \cdot 10^{14}\ \tfrac{\text{erg}}{\text{keV}^4\ \text{cm}^3} \end{aligned}$$

Figure 7 shows the material temperature computed after one time step with $\Delta t = 0.4$ ns for various values of the initial material temperature, $T_{m,0}$. As in the previous infinite medium problem, we see that the IMC method frequently results in an unphysical solution. The material temperature, T_m, is greater than the boundary source temperature T_B in nearly all of the cases tested for IMC. We see that this is not the case for IIMC, as $T_m < T_B = 1$ keV for all values of $T_{m,0}$ tested.

Although the IIMC method does not violate the maximum principle, the run time quickly becomes prohibitively costly as $T_{m,0}$ decreases, effectively increasing the initial opacity. Figure 8 shows how quickly the number of IIMC iterations required for just one time step grows. For high σ_a, nearly all of the emitted photons in each IIMC iteration are reabsorbed by the material. However, T^i, as calculated from Eq. (22), is the value of the temperature that would be achieved if none of the thermally emitted photons were reabsorbed. Thus, when the opacity is large, T^i is a very low estimate of T_{n+1}. Since T^i is small, the thermal emission on iteration i is small, and the absorption during iteration i is small. This means that the change in the absorbed energy is small, so T^{i+1} is only slightly larger than T^i. This results in extremely slow convergence for E_a, I_t^i, and T^i, which, in turn, results in slow convergence for the IIMC method overall. This increase in the number of iterations when the opacity is large is in accord with the behavior of the analytic problem described in Section 5.

To further illustrate how IIMC performs as $T_{m,0}$ decreases or as σ_a increases, we revisit Eq. (25). For the face source problem, with $e_m(T) = \rho c_v T$, Eq. (25) can be rewritten as

$$\rho c_V (T^i - T_n) = E_a^{i-1} - c\sigma_P a (T^i)^4 \Delta t \tag{41}$$

When we solve for T^i in this equation, we are essentially assuming that none of the emitted energy in the i-th IIMC iteration (which has a magnitude of $c\sigma_P a \left[(T^i)^4 - (T^{i-1})^4\right] \Delta t$) will be reabsorbed by the material. This gives us a value for T^i that is guaranteed to be greater than T^{i-1}. This is a desirable property, as it helps ensure that the T^i are monotonically converging to T^∞ from below. However, when σ_P is large, the assumption that none of the emitted energy is absorbed by the material is very much untrue and, as a result, T^i is a very poor approximation for T^∞.

Let us define p as the probability that an emitted photon that will escape re-absorption by the material. One technique we have considered to accelerate the IIMC process is the inclusion of p in Eq. (41) to get a better estimate for T^i, denoted as T^*:

$$\rho c_V (T^* - T_n) = E_a^{i-1} - c\sigma_P a (T^*)^4 \Delta t + (1-p) c\sigma_P a \left[(T^*)^4 - (T^{i-1})^4\right] \Delta t \tag{42}$$

Here, $p = 1$ would give us the lowest possible value of T^*, returning Eq. (42) to Eq. (41) and yielding the original T^i value. $p = 0$ would give us the highest possible value of T^*, an upper bound for T^∞. Figure 9 shows T^* plotted against p for $i = 0$, for three different problems: the face source problem with $T_{m,0} = 0.1$ and $T_{m,0} = 1$, and the first time step of the infinite medium problem from Section 7.2 with $\Delta t = 10^{-2}$. Note that the equation of state is the same in the infinite medium problem as it is in the face source problem, so Eq. (42) is valid for all three plots in Figure 9.

From the markers indicating T^∞ in Figure 9, we can see that, the smaller the value of p, the more difficult it is for a problem to converge. To see why this is the case, we can derive an approximation for the number of iterations required to converge. Let $\Delta E_a^i = E_a^i - E_a^{i-1}$. Then, if we interpret p as the fraction of the emitted energy that is not absorbed in each IIMC iteration, ΔE_a^i can be represented as a geometric sequence:

$$\begin{aligned}
\Delta E_a^{-1} &= E_a^{-1} \\
\Delta E_a^0 &= (1-p)\Delta E_a^{-1} \\
\Delta E_a^1 = (1-p)\Delta E_a^0 &= (1-p)^2 \Delta E_a^{-1} \\
&\dots \\
\Delta E_a^i &= (1-p)^{i+1} \Delta E_a^{-1} \\
&\dots
\end{aligned} \tag{43}$$

Thus,

$$E_a^\infty = \sum_{i=-1}^{\infty} \Delta E_a^i = \frac{E_a^{-1}}{1-(1-p)} = \frac{E_a^{-1}}{p} \tag{44}$$

Let n be the number of IIMC iterations required to achieve the convergence criterion. If the convergence criterion is given by

$$\frac{\Delta E_a^i}{E_a^i} \approx \frac{\Delta E_a^i}{E_a^\infty} < \epsilon \tag{45}$$

then setting $i = n$ and plugging in our definitions of ΔE_a^i and E_a^∞ yields

$$\frac{\Delta E_a^i}{E_a^\infty} = \frac{(1-p)^{n+1} E_a^{-1}}{E_a^{-1}/p} = p(1-p)^{n+1} < \epsilon \tag{46}$$

Taking the logarithm of both sides and rearranging the inequality to solve for n yields

$$n \geq \frac{\log \epsilon - \log p}{\log\,(1-p)} - 1 \tag{47}$$

Figure 10 shows the minimum n required to satisfy Eq. (47) as a function of p. This approximation of n grows very quickly as p gets small, and roughly scales as $1/p$. We note that Eq. 47 is a gross simplification of what actually occurs. This figure is only intended to illustrate how quickly n can grow as p shrinks and σ_a increases. In reality, E_a^i changes much more erratically due to statistical noise from the Monte Carlo simulation, and this affects both the accuracy and the convergence rate of the IIMC simulation.

If p is known exactly beforehand, solving for T^* in Eq. (42) would yield T^∞ exactly. We performed simulations in which we approximated p as the fraction of emitted energy in a zone that is not absorbed in that zone in the previous IIMC iteration. However, because a photon escape is such a rare event for large values of σ_P, it is difficult to get an accurate estimate of p without running an enormous number of particle histories. An overestimate of p would yield $T^* > T^\infty$; this would ruin the monotonic convergence of the T^i sequence, and result in negative weight particles. Future work will attempt to approximate p in a more sophisticated way, perhaps by using information on the size and shape of the zone and the average mean free path in the zone.

To significantly improve the convergence, it would be necessary to obtain an approximation of p that only slightly underestimates the actual value. As Figure 9 indicates, if p is underestimated by more than 2-3 orders of magnitude, convergence is improved only marginally, since T^* changes so sharply with p. If p is too close to the true value, however, it is easy for us to overestimate E_a^∞, since it is also very sensitive to changes in p.

7.4 Frequency-Dependent Face Source Problem

In this subsection, we consider a frequency-dependent face source problem from section V of Fleck and Cummings [3]. This problem has a frequency-dependent macroscopic absorption opacity given by Equation 5.1 [3]:

$$\sigma_a(T,\nu) = \frac{27\ \text{keV}^3\ \text{cm}^{-1}}{\left(\frac{\nu h}{k}\right)^3}(1 - e^{-\frac{\nu h}{kT}}) \tag{48}$$

The equation of state is given by

$$e_m(T) = \rho c_v T \tag{49}$$

where $\rho c_v = 8.1181 \cdot 10^{13} \frac{\text{erg}}{\text{keV cm}^3}$ is constant. This value is the same as that of ρc_v in the gray face source problem of Section 7.3.

The original problem from Fleck and Cummings used an initial material temperature of 0.001 keV, but, because IIMC is prohibitively slow for this case, we used the higher initial temperature

$T_{m,0} = 0.1$ keV for our simulations. As in the previous problem, the left boundary is a face source at 1.0 keV, at $x = 0$. The right boundary in this problem is a vacuum at $x = 4$ cm. $\Delta x = 0.4$ cm is used for the spatial mesh.

Spatial temperature profiles from IMC and IIMC for time steps of $\Delta t = 2 \cdot 10^{-4}$ ns and $\Delta t = 2 \cdot 10^{-1}$ ns are shown in Figures 11(a) and 11 at $ct = 3, 6$, and 12 cm. As in the Fleck and Cummings paper, ct is the time t multiplied by the speed of light c in order to convert it to a distance value. Note that, in Figure 11, one time step of $2 \cdot 10^{-1}$ ns results in a ct value of 6 cm, so there is no result for $ct = 3$ cm.

The results here are similar to those from the infinite-medium problem in Section 7.2. With a sufficiently small time step, as in Figure 11(a), the IMC and IIMC results agree well. The small differences between the IMC and IIMC results are due to statistical noise that could be further reduced by using more particles per time step and per IIMC iteration. However, if the time step grows too large, as in Figure 11, IMC becomes significantly more inaccurate than IIMC and eventually violates the maximum principle. We see that, even as the IMC simulation progresses to the next time step, the material temperature in the first zone remains unphysically high. In contrast, the IIMC simulations produce results that are thermodynamically consistent. The material temperature remains below both the source temperature and the radiation temperature at all times and locations.

Figures 12 and 13 show the distribution of photon frequencies from IIMC in two different scenarios. The histogram in Figure 12 was obtained by running IIMC for one time step of size $\Delta t = 2 \cdot 10^{-1}$ ns with slightly altered parameters from the frequency-dependent face source problem that has been described in this section. Instead of $T_{m,0} = T_{r,0} = 0.1$ keV, we have $T_{m,0} = T_{r,0} = 1$ keV. The right boundary was made reflective, and the domain was reduced to one spatial cell of size 0.4 cm. This problem starts out in equilibrium and, as expected, remains in equilibrium.

The histogram in Figure 13 was obtained by running IIMC for the regular frequency-dependent face source problem, with $T_{m,0} = T_{r,0} = 0.1$ keV, a domain stretching 4 cm, and a vacuum boundary on the right hand side. The histogram shown is obtained at the 8th time step, with $\Delta t = 2 \cdot 10^{-1}$ ns, where T_m and T_r are nearly in equilibrium at 0.955 keV and 0.935 keV, respectively.

Figures 12 and 13 demonstrate that the photons resulting from the iterations in Eq.(19) have the correct frequency. The source terms in this equation are the difference of Planckians at two different temperatures, but have the same frequency distribution, as discussed in the description of Eq.(16). So the photons resulting from the source terms in Eq.(19) have different energies. However, for a zone in which $T_r \approx T_m$, we should find that the frequency distribution of the sum of all of these photons will be a Planckian at the zone temperature. This is in fact the case for IIMC, as these figures illustrate.

CONCLUSIONS AND FUTURE WORK

We have described a new method of Monte Carlo thermal radiation transport. This method involves iterating on the matter temperature to make the solution of the transport equation implicit in this variable, unlike the standard IMC technique. We have named the method

Iterative Implicit Monte Carlo (IIMC). Because the method is fully implicit on the matter temperature, which is used to calculate the amount of thermal emission, the new method is not subject to the violations of the maximum principle that can occur with IMC.

The IIMC method requires us to construct a monotonically increasing sequence of approximations for the matter temperature. The values of this sequence are obtained by solving a non-linear equation for an estimate of the t_{n+1} temperature. This non-linear equation must be solved once for each zone in each iteration. This estimate takes into account thermal emission, but ignores the re-absorption of the thermally emitted photons simulated in each iteration. Ignoring the re-absorption ensures that the sequence of temperatures is monotonically increasing. However, in optically thick zones, this estimate can be much lower than the true t_{n+1} matter temperature. When this occurs, IIMC takes many iterations to converge to the t_{n+1} matter temperature. Because of the number of iterations required can be very large in problems with opaque zones, this new method in its current form does not appear to be competitive with IMC for those problems .

Future efforts will focus on reducing the number and expense of iterations required in optically thick problems. The number of iterations can be reduced by better estimating the t_{n+1} matter temperature. This can be done by using an estimate of the amount of thermal energy emitted in each zone which is reabsorbed in that zone. Ths estimate would be used in Eq.(22), and would result in a higher value of T^i. Higher values of T^i would presumably result in faster convergence and fewer iterations.

The expense of each iteration can be reduced by decreasing the number of particles used to represent thermal emission in each iteration. As the series in Eq.(19) converges, the amount of energy emitted in each iteration becomes smaller. In this work, we have used he same number of particles to model thermal emission in each iteration, which means that the energy weight of each particle decreases. Reducing the number of particles in each iteration in a manner that reflects the decrease in the energy emitted would reduce the expense of each iteration.

ACKNOWLEDGMENTS

This work performed under the auspices of the U.S. Department of Energy by Lawrence Livermore National Security, L.L.C. under Contract DE-AC52-07NA27344. The work of the second author was also supported under a Department of Energy Nuclear Energy University Programs Graduate Fellowship.

REFERENCES

1. G. C. Pomraning, "Equations of Radiation Hydrodynamics", in International Series of Monographs in Natural Philosophy, edited by D. ter Harr (Pergamon, New York, 1973), Vol. 54.

2. J. A. Fleck in "Computational Methods in the Physical Sciences" (B. Alder and S. Fernbach, Eds) Vol 1 p.43, McGraw-Hill, New York (1963).

3. J. A. Fleck, Jr., and J. D. Cummings, "An Implicit Monte Carlo Scheme for Calculating Time and Frequency Dependent Nonlinear Radiation Transport," *J. Comput. Phys.*, **8**, pp. 313-342 (1971).

4. N. A. Gentile, "Including the Effects of Temperature-dependent Opacities in the Implicit Monte Carlo Algorithm," *J. Comput. Phys.*, **230**, pp. 5100-5114 (1971).

5. N. A. Gentile, N. Keen, and J. Rathkopf, "The Kull IMC Package", Technical Report UCRL-JC-132743, Lawrence Livermore National Laboratory, Livermore, CA (1998)

6. W. H. Press, et. al, "Numerical Recipes, Second Edition", Cambridge University Press, New York, N. Y., (2002)

7. E. W. Larsen and B. Mercier, "Analysis of a Monte Carlo Method for Non- linear Radiative Transfer," *J. Comput. Phys.* **71**, 50 (1987).

8. E. D. Brooks, "Symbolic Implicit Monte Carlo", *J. Comput. Phys.* **83**, 433 (1989).

9. J. R. Cheatham, Ph. D. Thesis http://deepblue.lib.umich.edu/bitstream/2027.42/75852/1/cjesse 1.pdf (2010)

10. A. R. Long, N. A. Gentile, and T. S. Palmer, "The Iterative Thermal Emission Method: a More Implicit Modification of IMC", submitted to *J. Comput. Phys.*

11. Bingjing Su and Gordon L. Olson, "Am Analytical Benchmark for Non-equilibrium Radiative Transfer in an Isotropically Scattering Medium," *Ann. Nucl. Energy* **24**, pp. 1035-1055 (1997).

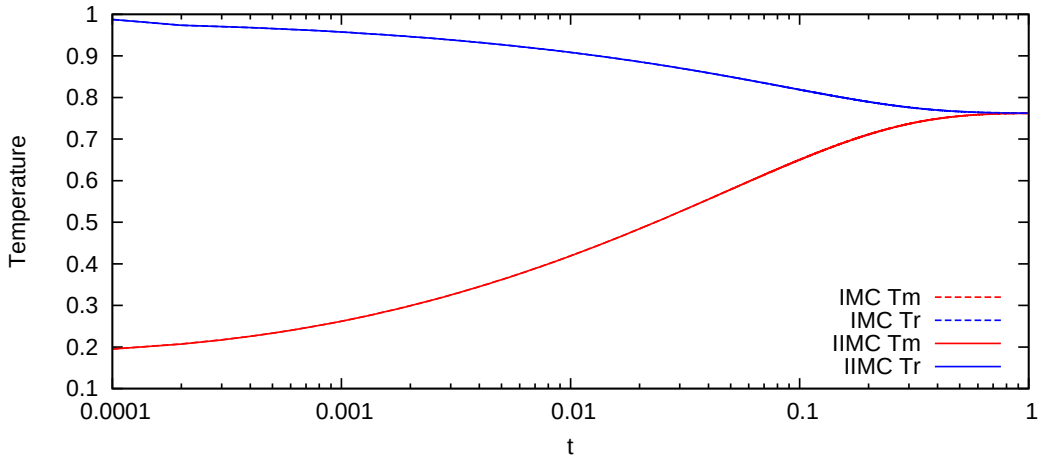

(a) $\Delta t = 10^{-4}$

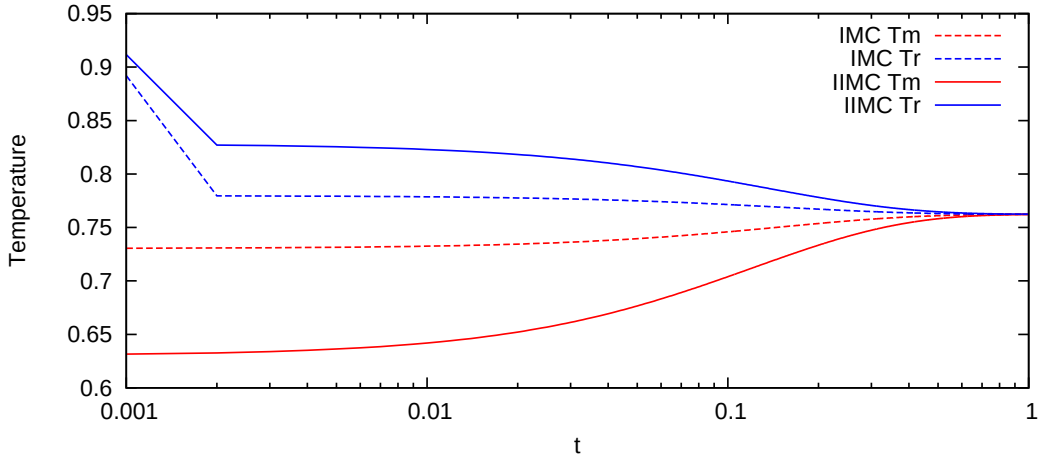

(b) $\Delta t = 10^{-3}$

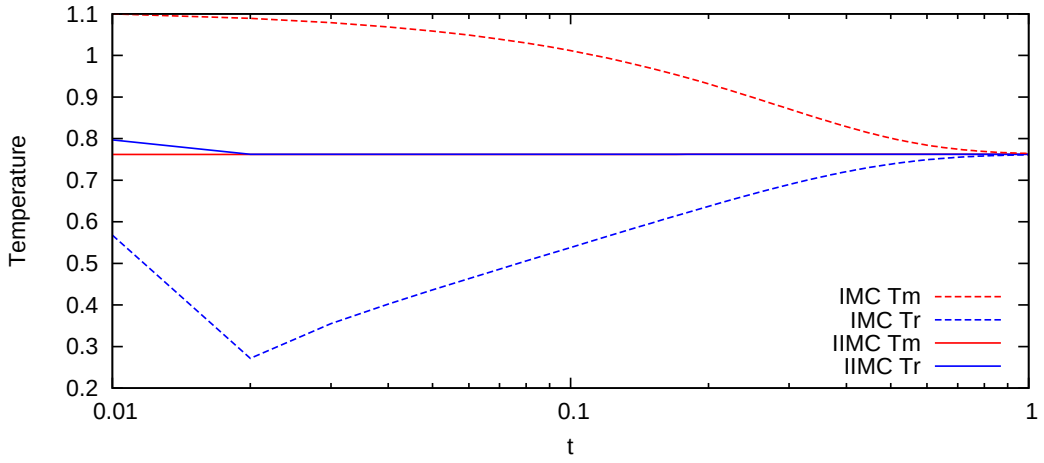

(c) $\Delta t = 10^{-2}$

Figure 6: Comparison of IMC and IIMC for the one-zone problem described in Section 7.2 for various Δt.

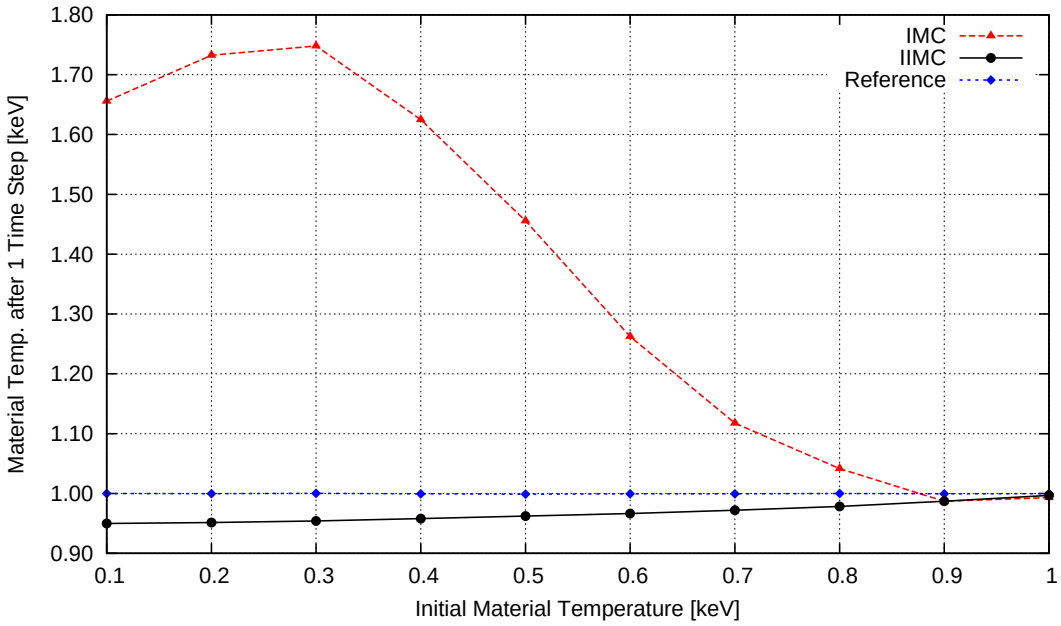

Figure 7: Temperature after 1 time step for the face source problem described in Section 7.3 using IIMC and IMC with $\Delta t = 0.4$ ns. The reference solution values are calculated using an IMC simulation at $t = 0.4$ ns with $\Delta t = 4 \cdot 10^{-5}$ ns.

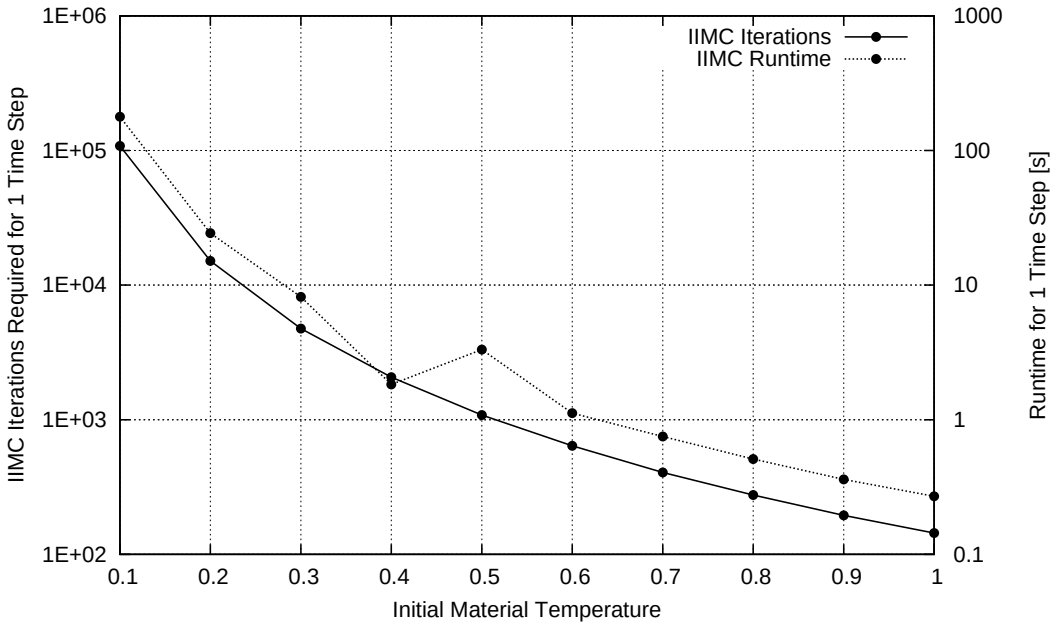

Figure 8: Number of IIMC iterations and run time required for the first time step vs. starting material temperature for the face source problem described in Section 7.3. Here, $\Delta t = 0.4$ ns. As the difference between T_m and the face source temperature increases, IIMC quickly becomes very expensive. Note that no data exists between the markers. The lines connecting the markers are only there as a visual aid.

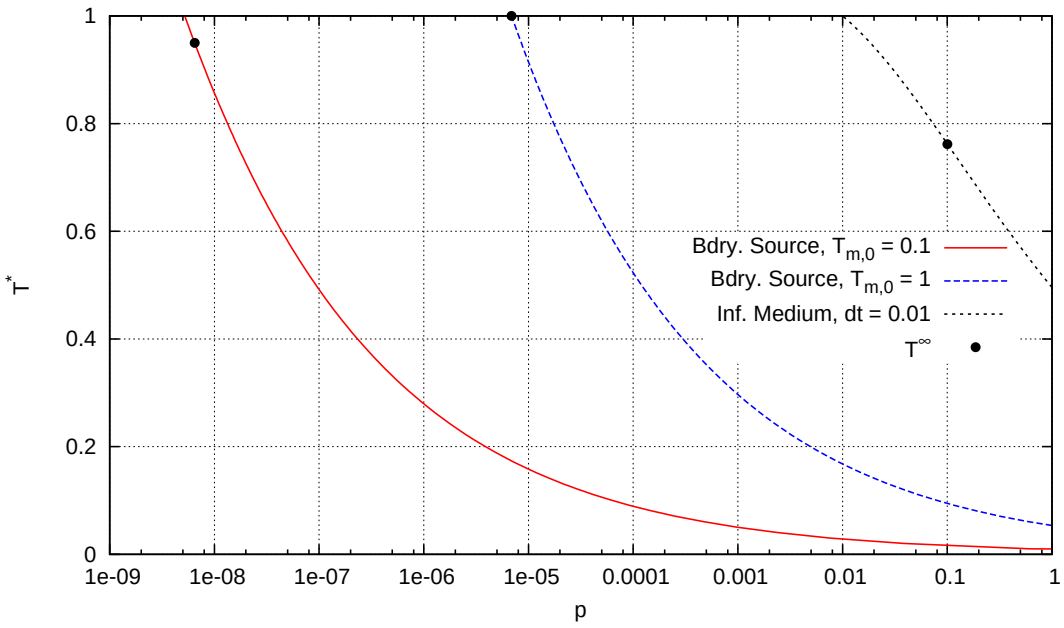

Figure 9: Eq. 42 plotted for $i = 0$ for three different problems. The plots denoted $T_{m,0} = 0.1$ and $T_{m,0} = 1$ are from the face source problem in Section 7.3 with starting material temperatures of 0.1 and 1.0, respectively. The plot denoted "Inf. Medium" is from the first time step of the infinite medium problem in Section 7.2, with a time step of 10^{-2}. The black dots indicate the temperature that IIMC converges to for that particular problem after one time step.

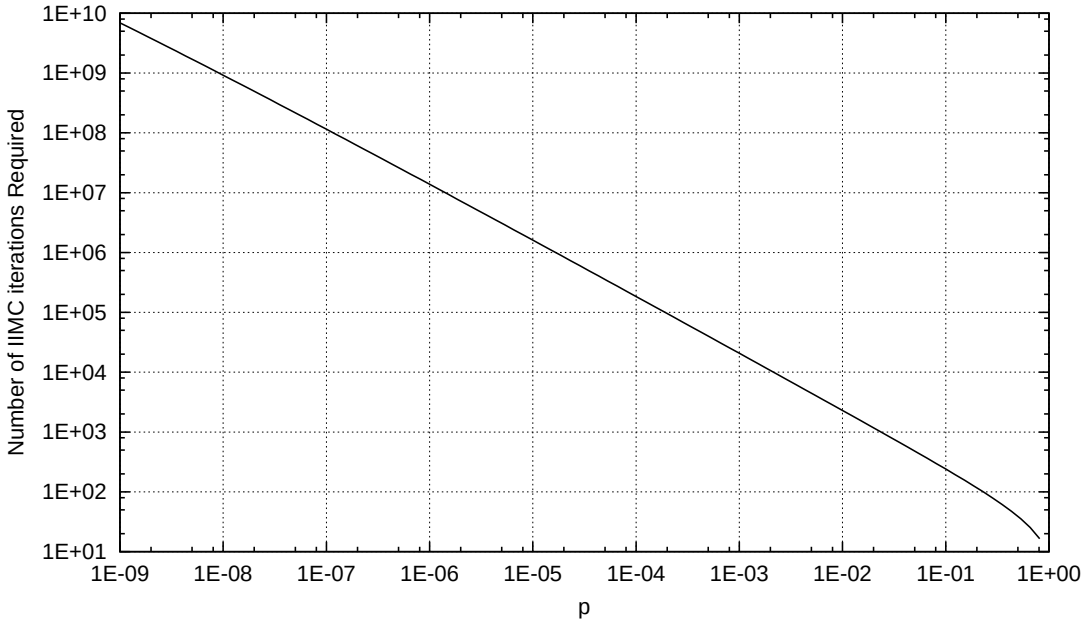

Figure 10: Approximate number of IIMC iterations required to complete a time step vs. p, the probability that a photon emitted in an IIMC iteration escapes re-absorption by the material. See Eq. (47).

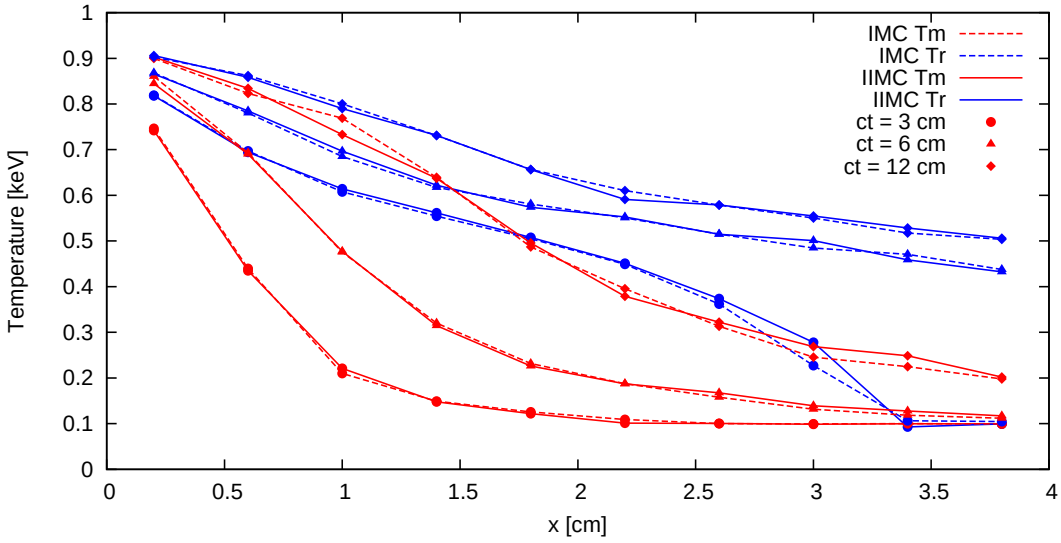

(a) $\Delta t = 2 \cdot 10^{-4}$ ns

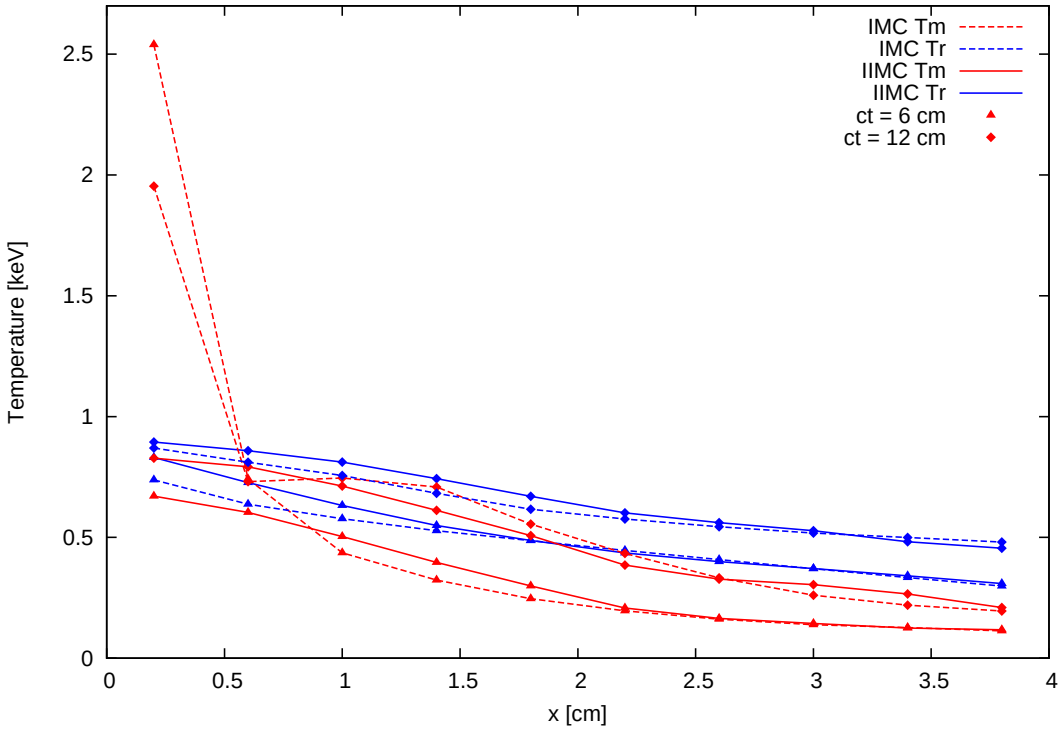

(b) $\Delta t = 2 \cdot 10^{-1}$ ns

Figure 11: Spatial material and radiation temperature distributions at various values of t for the frequency-dependent face source problem in Section 7.4. Results from both IMC and IIMC are shown using two different values of Δt. The times are given as ct, which is simply the time t multiplied by the speed of light c. Note that $\Delta t = 2 \cdot 10^{-1}$ ns corresponds to $\Delta(ct) = 6$ cm, so there is no $ct = 3$ cm result for that time step size.

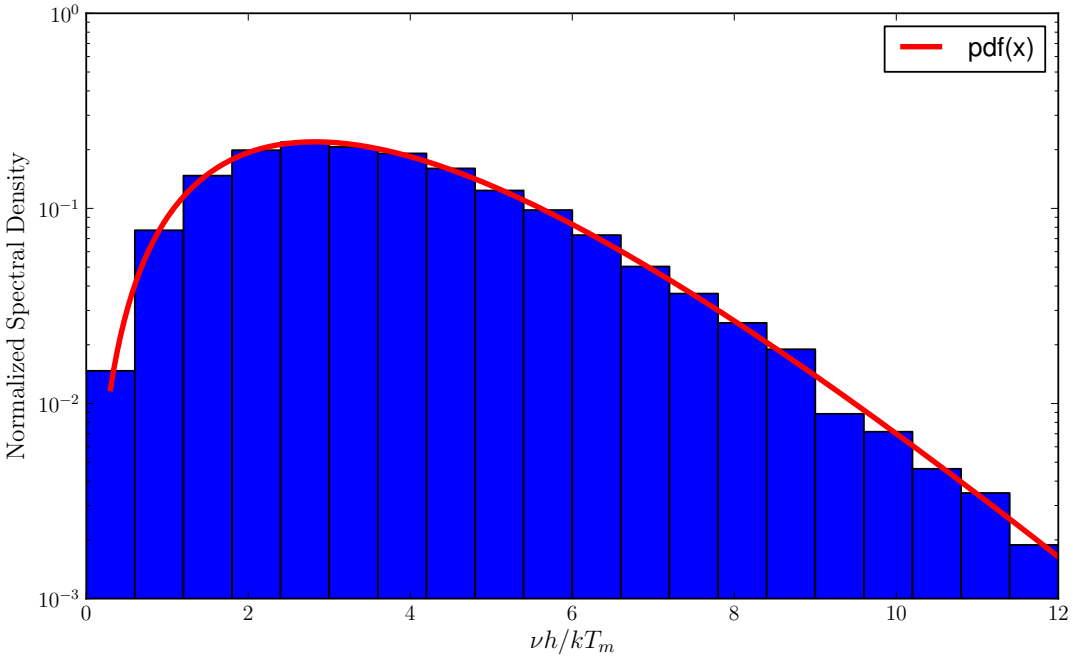

Figure 12: Normalized frequency distribution for problem with an absorption opacity given by Eq. (48), after one time step of size $\Delta t = 2 \cdot 10^{-1}$ ns. This problem is described in Section 7.4 as a variant of the usual frequency-dependent face source problem. It has $T_{m,0} = T_{r,0} = 1$, a reflective right boundary, and its domain is shrunk to just one spatial cell of size 0.4 cm.

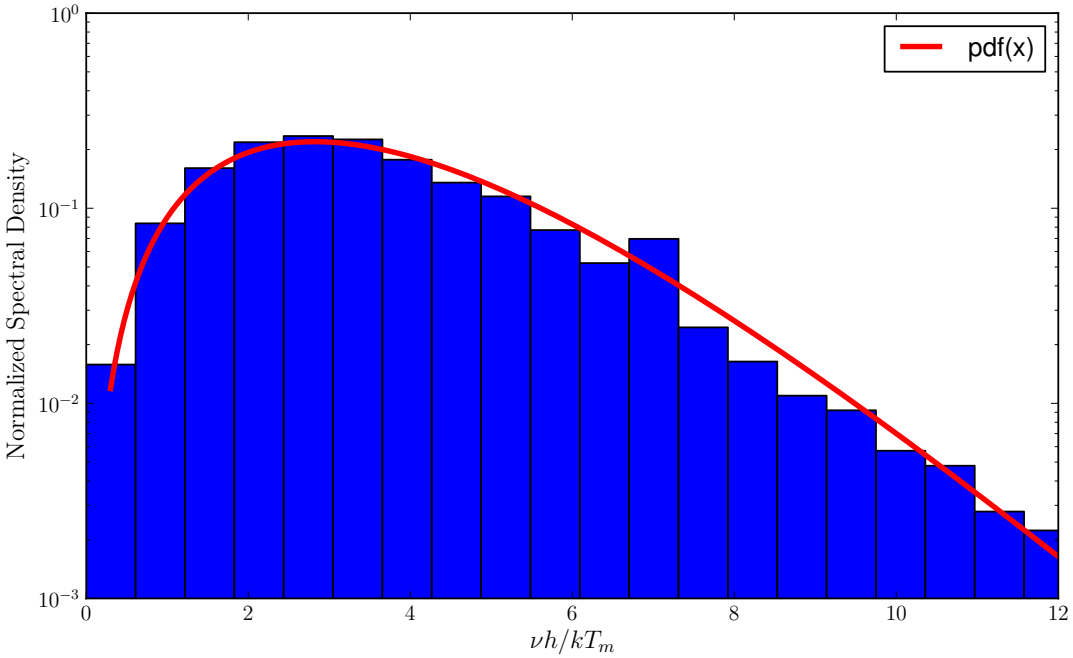

Figure 13: Normalized frequency distribution in the first zone (centered around $x = 0.2$ cm) for frequency-dependent face source problem described in Section 7.4, after 8 time steps of $\Delta t = 2 \cdot 10^{-1}$ ns ($ct = 48$ cm). In this zone at this time, we have $T_m = 0.955$ keV and $T_r = 0.935$ keV.